

MM Science Journal | www.mmscience.eu

ISSN 1803-1269 (Print) | ISSN 1805-0476 (On-line)

Special Issue | HSM 2025

18th International Conference on High Speed Machining October 15-16, 2025, Metz, France

DOI: 10.17973/MMSJ.2025_11_2025146



HSM2025-45121

SIMULATION-BASED ANALYSIS OF TOOL WEAR PROGRESSION AND MECHANISMS IN TITANIUM ALLOY MACHINING

N. Zhang^{1*}, F. Kneubühler¹, H. Klippel¹, K. Wegener^{1,2}

¹inspire AG, Technoparkstrasse 1, 8005, Zurich, Switzerland

²ETH Zurich, D-MAVT, Leonhardstrasse 21, 8092, Zurich, Switzerland

*Corresponding author; nanyuan.zhang@inspire.ch

Abstract

This study presents a simulation-based approach for analyzing tool wear progression in Ti6Al4V machining using an in-house developed hybrid Smoothed Particle Hydrodynamics—Finite Element Method (SPH-FEM) solver. Cutting experiments are used to examine key wear indicators including crater depth and flank wear land width along with SEM analysis to understand underlying wear mechanisms. Despite the dominance of diffusion-accelerated attritious wear in titanium machining, the phenomenological Usui model is selected for wear simulation. Within a two-dimensional chip formation framework, the wear algorithm is integrated at the end of each time increment to predict wear progression based on tool—chip and tool—workpiece contact conditions. A correlation between relative wear rates and the Arrhenius law coefficient across varying cutting speeds is identified through simulation, providing the foundation for a new calibration method tailored to the Usui wear model. The calibrated models are then applied back within the same simulation framework for validation, demonstrating good predictive accuracy and strong agreement with experimental trends, particularly for crater wear.

Keywords:

tool wear, simulation, SPH, FEM, titanium alloy

1 INTRODUCTION

Tool wear results from complex mechanical, chemical, and thermal interactions between the cutting tool and the workpiece, critically influencing machining quality, tool life, and manufacturing costs. Different workpiece materials result in distinct wear behaviors, requiring careful study to optimize cutting parameters and tool geometries. Titanium alloys such as Ti6Al4V are particularly challenging to machine due to their tendency to cause severe wear, which is primarily driven by high cutting temperature, chemical reactivity, and a strong affinity to oxygen [daSilva 2019, Lindvall 2021].

Generally, tool wear can be categorized into macroscopic and microscopic scales. Macroscopic wear refers to visible damage such as deformation, chipping, or fracture. In contrast, microscopic wear mechanisms, which are more commonly studied, include abrasion, adhesion, diffusion, oxidation, and other forms of surface degradation. These mechanisms result in characteristic wear patterns, such as crater wear on the rake face and flank wear land on the flank face. Accurate modeling of tool wear is essential, as it enables the prediction of wear rates and tool lifespan, allowing for reliable process planning and tool design without relying solely on time-consuming experimental trials. Flank wear land width VB and crater depth KT are two of the most used indicators for evaluating tool life, and

most wear models are developed to predict the progression of these indicators. The Usui wear equation [Usui 1984], one of the most widely adopted models, relates the local wear rate to contact pressure σ_n , sliding velocity v_{rel} and temperature T at the local contact interface:

$$\dot{w} = C_1 \sigma_n v_{rel} \exp\left(-\frac{C_2}{T}\right) \tag{1}$$

Originally developed for abrasive and adhesive dominated mechanical wear, the Usui model has demonstrated its validity across various machining applications, including carbon steels, low-alloy steels, and titanium alloys. In this model, the coefficient \mathcal{C}_2 in the Arrhenius term is typically interpreted as a combined representation of adhesion-related activation energy, material hardness, and potentially other surface phenomena, such as the formation and thinning of oxide layers. Since direct physical determination of this parameter is difficult, it is thus often treated as a fitting constant.

Calibration of tool wear models can be performed using either experimental data or numerical simulations. In experimental calibration, worn tool profiles from machining tests are commonly used to derive model constants. This approach relies on measuring key physical variables at the tool-chip and tool-workpiece interfaces, including temperature, sliding velocity, and normal contact pressure. While sliding velocity can be estimated analytically,

accurate contact pressure and temperature data is rather challenging to obtain. On the rake face, contact pressure can be reliably measured using methods like the split-tool technique. On the flank face, it is often assumed to be uniformly distributed and derived from process forces [Malakizadi 2016]. Temperature value is typically measured using methods such as thermocouples or thermal cameras [Davies 2007]. However, due to limitations in spatial resolution and the inaccessibility of the contact interface, these methods may fail to capture the peak physical values at the interface, thereby introducing uncertainty into the wear model calibration [Zhang 2024].

To overcome the challenges associated with directly measuring physical contact conditions, numerical simulations are increasingly employed to extract the required physical contact variables [Haddag 2013, Bencheikh 2020]. In this approach, worn tool geometries obtained either through manual modeling or high-resolution microscopy are embedded into chip formation simulations, and thus the physical contact variables are extracted for the wear model calibration [Schulze 2011, Malakizadi 2016]. While this method improves the accuracy of contact variable estimation due to the close match with the actual tool geometry, its calibration efficiency is limited by the discrete representation of tool life and the need for repeated simulations at multiple wear states.

In addition to using given cutting tool geometries to simulate chip formation and extract physical contact variables, directly simulating tool wear evolution presents another possibility for both wear prediction and model calibration. A foundational approach was established through the development of a wear simulation framework that integrates user-defined wear algorithms into chip formation simulations using commercial software. Introduced in early studies using the DEFORM 2D [Yen 2002], this approach divides the tool life into discrete wear increments, during which thermomechanical variables at the contact obtained from chip formation simulation are used to calculate the corresponding wear volume. The tool geometry is then updated and applied in the subsequent chip formation simulation, enabling a stepwise representation of wear progression. This approach has remained the core principle of wear progression simulation for nearly two decades and has been adopted by many researchers [Xie 2005, Lorentzon 2008, Attanasio 2010, Zanger 2013, Binder 2017]. However, the advancement of wear progression simulation has been constrained by the limitations of commercial software, which restrict both modeling flexibility and computational efficiency. Particularly, using finer wear increments requires repeatedly performing chip formation simulations, significantly increasing the computational cost and limiting the practical coupling of wear evolution with the cutting process. To overcome this limitation, a recently inhouse developed SPH-FEM solver [Zhang 2023b] has been applied to perform wear progression simulations [Zhang 2023a], where the wear-related calculations are embedded at the end of each time increment during the chip formation simulation. This approach enables tight integration of the wear calculation into a single set of cutting simulation, allowing for efficient modeling of tool wear evolution.

In this work, the SPH-FEM framework is applied to simulate the wear behavior of carbide tools in Ti6Al4V machining, with the objective of developing a new wear model calibration method based on the simulated wear progression. Section 2 presents the cutting experiments along with the observed wear patterns and corresponding mechanism analysis, followed by the simulation setup in Section 3. The calibration methodology and results are

discussed in Section 4, and the main conclusions are summarized in Section 5.

2 AUXILIARY CUTTING EXPERIMENTS

2.1 Setup of cutting experiments

A total of 17 quasi-orthogonal cutting tests on Ti6Al4V were performed using a Schaublin 42L CNC lathe to investigate cemented carbide tool wear and to identify appropriate wear models for Ti6Al4V machining. The workpieces were prepared as hollow cylinders with a wall thickness of 2 millimeters and mounted on the spindle. Uncoated cemented carbide inserts, WC with 6% Co (type CCMW 09T304 H13A, Sandvik Coromant), were mounted on a tool holder, which was fixed to a Kistler 9129AA dynamometer for force measurements. The experimental setup is illustrated in Fig. 1(a). All tests were conducted under dry conditions. The initial cutting edge radii of the inserts, measured using a Sensofar® S neox optical microscope and identified using Wyen's three-point method [Wyen 2012], ranged from 15 to 70 micrometers with an average value of 36.6 µm. The edges were subsequently precisionground to a uniform radius of 3.5 micrometers, with constant rake and clearance angles of 0° and 4.5°, respectively. The surface hardness of the tool after edge preparation averaged 1561 HV10. The cutting speeds varied between 150 and 350 m/min, with a constant uncut chip thickness of 0.1 mm. Different cutting distances were employed to evaluate tool wear progression, with each test using an unused cutting edge on the inserts. The process parameters are summarized in Tab. 1. In this paper, force measurements are used solely to demonstrate the consistency of the cutting tests. The signals were filtered using a 40 Hz cut-off frequency and normalized by cutting width to yield force values in N/mm. The consistent increase in cutting force with tool wear progression, observed across repeated tests at different cutting distances, indicates good repeatability of the experiments. An example of the processed force signals under a same cutting speed of 200 m/min is given in Fig. 1(b).

Tab. 1: Quasi-orthogonal cutting parameters.

Cutting speed v_c [m/min]	Uncut chip thickness <i>h</i> [mm]	Cutting distance <i>d</i> [m]	
150	0.1	1.00, 9.92, 16.02, 18.79	
200	0.1	1.00, 3.00, 6.01, 10.01, 15.87	
250	0.1	0.99, 2.98, 5.95, 9.92, 11.90	
300	0.1	1.00, 3.97, 8.93	

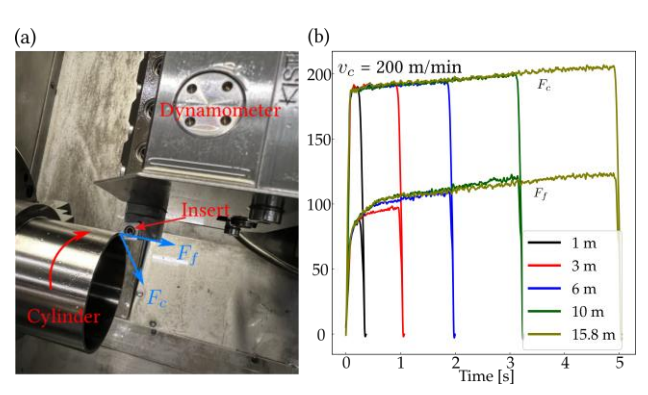


Fig. 1: (a) Illustration of the setup used for quasi-orthogonal cutting experiments, (b) exemplary force measurement results at a cutting speed of 200 m/min.

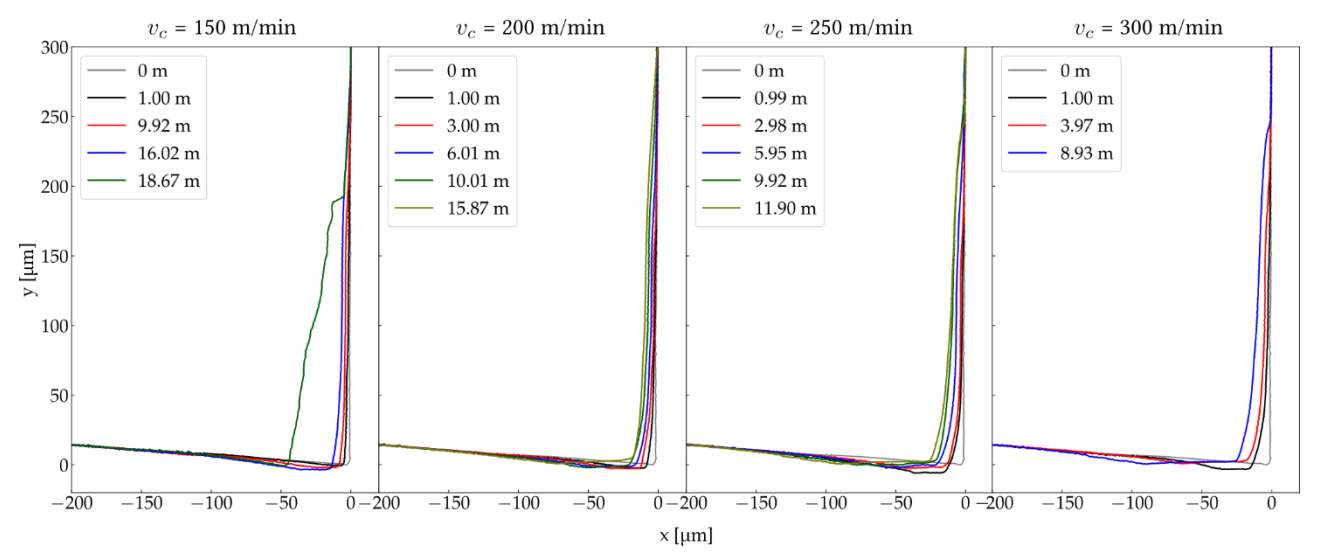


Fig. 2: Cross sections of etched cutting tools after machining.

2.2 Evaluation of wear progression

To examine the worn tool geometry and measure wear indicators after machining, the inserts were etched in a solution containing 20% oxalic acid (HO $_2$ C-CO $_2$ H) and 0.5% EDTA (ethylenediaminetetraacetic acid) at 75°C for four days. This solution was selected in order to minimize cobalt leaching from the cemented carbide during the etching, as recommended by Meier [Meier 2020]. The worn tool surfaces were examined under the same optical microscope mentioned before for contour measurement, as well as Scanning Electron Microscopy (SEM) for detailed microstructural analysis. Cross-sections of the worn tools, averaged over a width of approximately 15 μ m to produce smoother contours, are presented in Fig. 2.

Typical wear features including crater wear on the rake face and flank wear land on the flank face were consistently observed. In addition, severe plastic deformation around the cutting edge emerged as a prominent wear phenomenon, characterized by noticeable compression of the tool material from the rake face. This deformation is evident after as little as 1 m of cutting across all tested cutting speeds and often preceded the formation of a distinct crater. This plastic deformation likely accelerates the development of the flank wear land. Crater geometry is not symmetric, and the retreat of crater boundaries near the cutting edge complicates the measurement of crater depth values. In cases where a distinct crater center was not evident, it is approximated using the curvature inflection point. The measured KT and VB values are plotted in Fig. 3 to illustrate their progression with increasing cutting distances. Although plastic deformation introduces additional uncertainties in the progression of tool wear indicators particularly at higher cutting speeds, both KT and VB values exhibit strong linear relationships with the cutting length. This suggests that constant wear rates for KT and VB can be reasonably determined. The fitted wear rate results are also presented in Fig. 3.

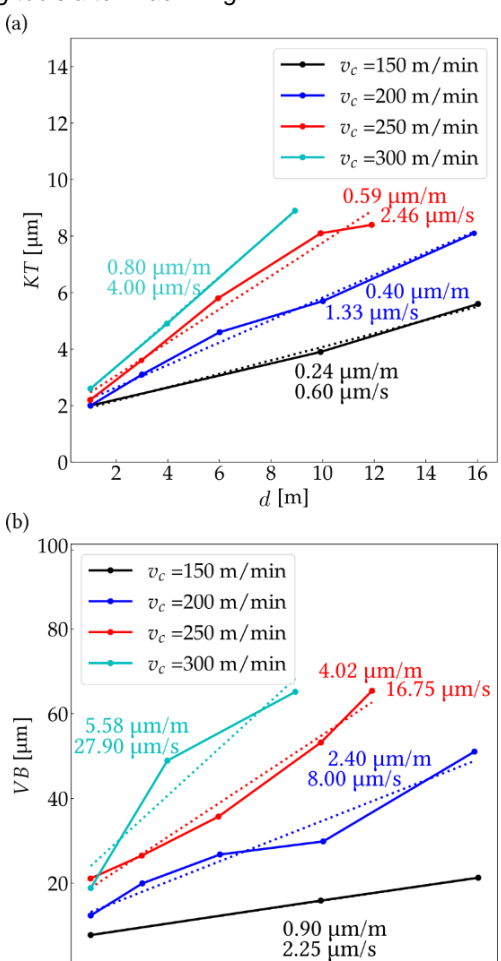


Fig. 3: Development of (a) KT and (b) VB from experiments along with the corresponding fitted wear rates.

8

d [m]

10 12 14

The worn tool surfaces typically appear smooth after etching. As an example, Fig. 4(a) shows the worn tool from a test run up to a cutting distance of 6.01 m with the cutting speed of 200 m/min, highlighting four key regions captured by SEM for further discussion: three on the rake face and one on the flank face. In the area near the cutting edge on the rake face illustrated in Fig. 4(b), abrasive marks from edge preparation remain visible, indicating minimal relative

motion between the tool and chip, and consequently limited material removal. Although some diffusion marks are present, grain pull-out appears minimal. Considering that this deformation is present even after 1 m of cutting, it can be confirmed that the geometry change around the cutting edge is primarily due to the plastic deformation instead of the microscopic tool wear. At the center of the crater shown in Fig. 4(c), diffusion is pronounced, especially around cobalt pockets, where the removal of small tungsten carbide grains results in the formation of coral-like surface structures. Due to space limitations, the EDS images are not included in this manuscript; however, detailed results are available in the author's thesis [Zhang 2024]. The analysis reveals a significantly higher concentration of Ti and O within the Co pockets compared to the surrounding WC grain areas, providing strong evidence for localized diffusion and oxidation processes. In the region around the end of the tool-chip contact zone in Fig. 4(d), a thin layer of deposited material is observed. It is composed of irregularly shaped grains with a characteristic size around 0.1 µm, which are particularly evident around the edges of cobalt pockets. These grains were likely transported from the crater region by the sliding chip and subsequently deposited in this area. On the flank wear land, as shown in Fig. 4(e), abrasive wear is the dominant mechanism. While plastic deformation is evident and a laminar tungsten carbide grain structure is observed, there is no clear evidence of diffusion. This is further confirmed by the EDS results presented in [Zhang 2024]. Due to plastic deformation and surface structure, the identification of grain pull-out in this region is difficult.

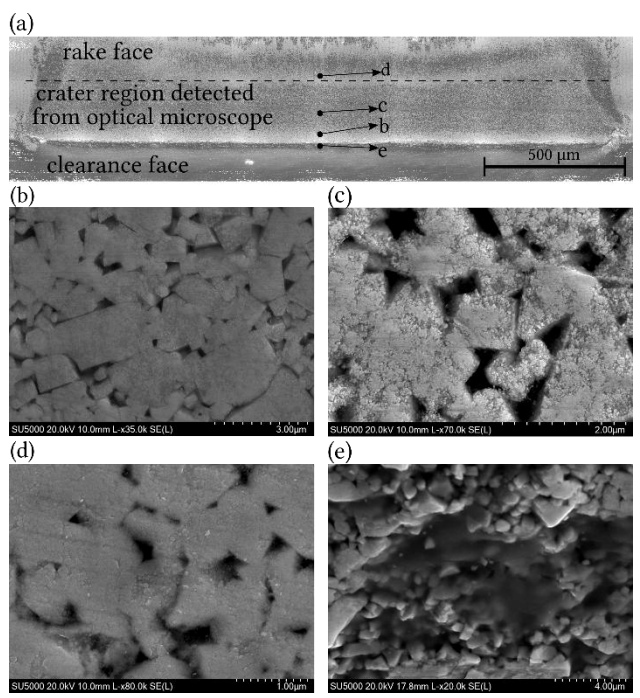


Fig. 4: Illustration of tool surfaces after Ti6Al4V cutting test with cutting speed of 200 m/min and cutting distance of 6.01 m. (a) Optical microscope result of the worn tool, (b) - (e) SEM images captured at the location marked in (a), with (b)-(d) showing different regions on the rake face, and (e) representing the area from the flank wear land.

2.3 Discussion of tool wear mechanism

In Ti6Al4V machining, distinct wear mechanisms act on the rake and flank faces of the carbide tool. On the rake face, diffusion- and oxidation-assisted attrition is the dominant wear mode, while mechanical wear prevails on the flank

face with limited diffusion involvement. The wear process involves titanium diffusion into WC grains and cobalt binder regions, contributing to microstructural degradation and microcrack formation [Zhang 2024]. These effects facilitate fine-scale material removal, leading to the formation of a relatively smooth crater surface. Sub-micron grain fragmentation and coral-like surface features are commonly observed, reflecting the progressive pattern of attrition-driven wear.

Despite the significant role of diffusion, the fundamental wear process remains attrition-based, involving adhesion, pull-out, and abrasion. Diffusion primarily acts to weaken the tool microstructure and facilitate localized material removal. Given that the Arrhenius formulation can be interpreted more broadly to encompass a range of thermally activated processes, the phenomenological Usui wear model which expresses wear rate as a function of mechanical power density $\sigma_n v_{rel}$ modulated by temperature through an Arrhenius term remains applicable for modeling crater wear in Ti6Al4V cutting. The calibrated coefficients in the Usui model therefore reflect a combined influence of mechanical, diffusive, and chemical effects, rather than strictly representing classical activation energy or material hardness. This broader interpretability offers a strong rationale for adopting the Usui model to represent the wear rate and to serve as the foundation for the model calibration performed in the current study.

3 SETUP OF CHIP FORMATION AND WEAR PROGRESSION SIMULATION

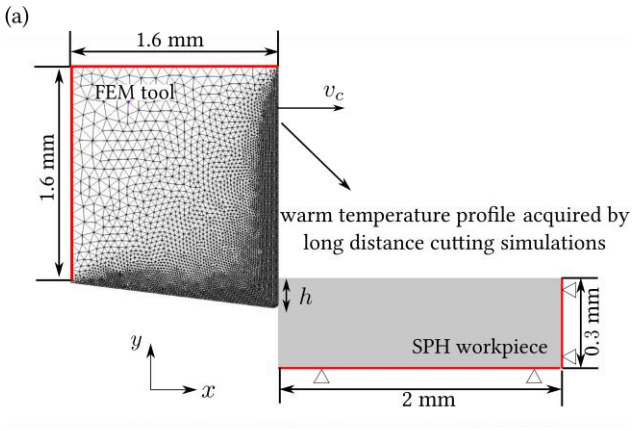
The setup for the hybrid SPH-FEM chip formation simulation is illustrated in Fig. 5(a). The workpiece is discretized into SPH particles, which enables robust thermomechanical analysis for large deformations while avoiding mesh distortion issues. The uncoated cemented carbide tool is modeled as a rigid yet thermally conductive body using a finite element mesh, allowing for efficient heat transfer calculations. The particle distance is set to 1.44 µm for the workpiece, which is sufficient for representing the deformation gradient in the shear band [Röthlin 2019]. A linear triangular mesh is employed to discretize the cutting tool. The finite element mesh size varies from 2 to 120 µm depending on the proximity to the tool-chip interface. The simulation model is designed to be compatible with Graphics Processing Unit (GPU) acceleration for faster calculations. To quickly reach the steady thermal state of the modeled tool-workpiece system and thus reduce the influence of temperature change on the simulated results, the FEM tool is specified with a warm temperature profile obtained from a repetitive long-distance cutting simulation over 22.0 mm, using a constant coefficient of friction (COF) of 0.35 [Zhang, 2023b].

The Johnson-Cook (JC) hardening law

$$\sigma_{y}^{JC}\left(\bar{\varepsilon}_{pl}, \dot{\bar{\varepsilon}}_{pl}, T\right) = \left[A + B\left(\bar{\varepsilon}_{pl}\right)^{n}\right] \left[1 + C \ln\left(\frac{\dot{\varepsilon}_{pl}}{\dot{\varepsilon}_{0}}\right)\right] \left[1 - \left(\frac{T - T_{r}}{T_{m} - T_{r}}\right)^{m}\right] \tag{2}$$

is used to describe the plastic behavior of Ti6Al4V, while a constant Coulomb friction model is used in the simulations. Since the material's shear response is inherently captured by the constitutive equations, the friction model is not constrained by the material's shear flow stress. The JC model parameters, workpiece and tool material properties and contact parameters used in simulations are listed in Tab. 2. Specifically, JC parameters of the workpiece Ti6Al4V are calibrated by inverse method using the cutting simulation [Klippel 2021]. The Taylor-Quinney coefficient χ

which represents the ratio of plastic work converting to heat is set to 0.9. Exemplary results of simulated chip formation without wear algorithm are given in Fig. 5(b), which demonstrates that the simulation can effectively capture the segmented chip in high speed machining of Ti6Al4V.



— boundary with fixed temperature T_0 =300K

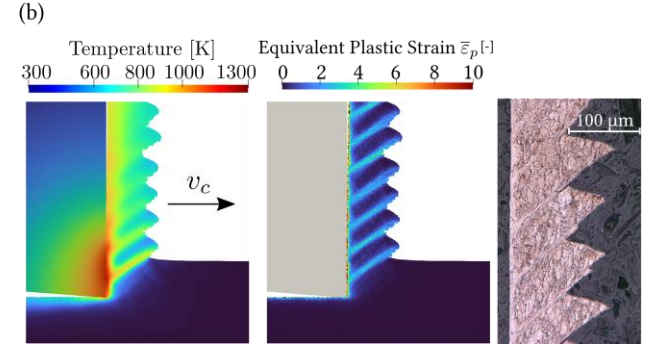


Fig. 5: (a) Configuration of the hybrid SPH-FEM chip formation simulation, (b) exemplary results of simulated temperature and equivalent plastic strain fields and experimental etched chip with v_c of 200 m/min.

Tab. 2: Johnson-Cook model parameters, material properties and contact parameters applied in simulation.

Johnson-Cook model parameters for Ti6Al4V							
A [MPa]	B [MPa]	<i>C</i> [-]	m [-]	n [-]	$\dot{ar{arepsilon}_0}$ [s $^{ extsf{-}1}$]	<i>T_r</i> [K]	<i>T_m</i> [K]
852.1		0.02754		0.148	1.0	300	1836
Material Properties			Ti6Al4V		WC (Co)		
Density ρ [kg/m ³]			4430		15250		
Young's modulus E [GPa]			110		-		
Poisson ratio ν [-]			0.35		-		
Specific heat c_p [J/(kg·K)]			526		292		
Thermal conductivity k [W/(m·K)]			6	8.8		88	

Contact parameters between tool and workpiece / chip			
Coefficient of friction (COF) μ [-]	0.35		
Frictional heat partition coefficient to tool eta_{fri} [-]			
Frictional energy converted to heat η [-]			
Heat transfer coefficient at the contact h_c [W/(m²·K)]			

The flowchart of the wear progression simulation is shown in Fig. 6(a). The wear algorithm is embedded at the end of each time increment in the chip formation simulation, where the local wear rate is calculated using the selected model, and tool geometry is updated via nodal displacement

IZhang 2023al. For carbide tools in Ti6Al4V machining, the Arrhenius coefficient in the Usui wear model typically ranges from 2500 to 20000 [Ozel 2010, Zanger 2013]. Regarding the diffusion process at the contact, the individual activation energy values for element diffusion of W, Co, and C from cemented carbide tools into the chip material and thus the coefficients used in the Arrhenius law are 37743.56, 40259.80, and 16103.92 respectively [Zhang 2009]. Considering the stronger association of Co and C with diffusive wear during titanium machining [Lindevall 2021], their corresponding coefficients, along with three additional representative values of 2,500, 5,000, and 10,000, are selected as C_2 values in the Usui model for the sensitivity analysis. In total, 25 simulations were conducted, covering five different \mathcal{C}_2 values across five cutting speeds, including an additional case at 350 m/min.

In the wear progression simulation, the Usui wear rate is scaled with a factor A':

$$\dot{w} = A' C_1 \sigma_n v_{rel} \exp\left(-\frac{C_2}{T}\right) \tag{3}$$

with A' set greater than 1 to accelerate wear progression, allowing the simulation to capture tool wear over extended cutting distances within a feasible computational time. For example, if the chip formation simulation covers 1.0 mm of cutting length within the steady thermomechanical states, setting A' as 1000 corresponds to simulating the wear progression over a cutting distance of 1 m. A representative simulated worn tool profile is shown in Figure 6(b), where both crater wear and the flank wear land are well captured.

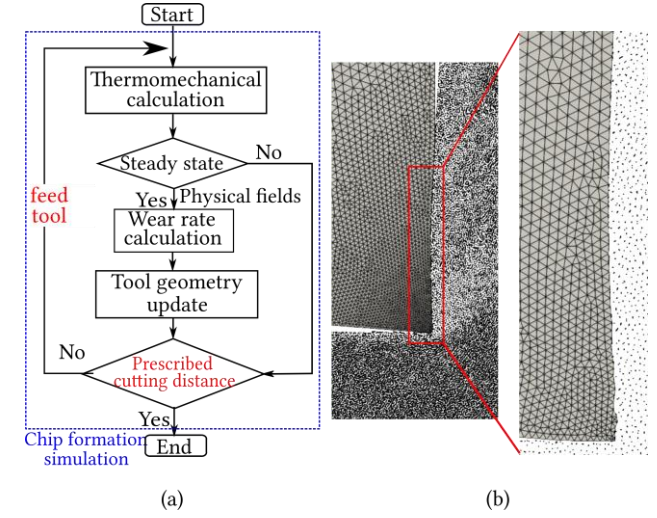


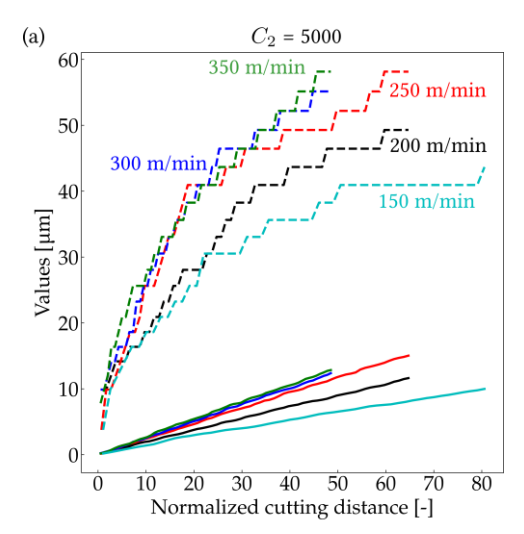
Fig. 6: (a) Flow chart of wear simulation within a chip formation simulation, (b) exemplary simulated tool wear profiles with close-up views of the worn tool surfaces.

4 RESULTS OF WEAR SIMULATION AND WEAR MODEL CALIBRATION

4.1 Simulated wear progression in Ti6Al4V cutting

Fig. 7 illustrates the comparison of relative simulated KT and VB values at different cutting speeds while employing the Usui wear model with two exemplary C_2 coefficients. This comparison facilitates understanding of how the C_2 parameter influences tool wear under varying cutting conditions. Note that since C_1 is unknown, different values of A' were used to control the wear volume generated in each time increment. As a result, the cutting distance has been normalized to enable meaningful comparison across different cutting speed cases. The simulated KT values exhibit a nearly constant rate of increase of cutting distance, while the piece-wise curves of VB indicate varying wear

rates, possibly reflecting an initial wear phase followed by a more stable wear stage. Importantly, a higher \mathcal{C}_2 leads to more pronounced variations in wear rates with changes in cutting speed. This observation can be attributed to the increased temperature sensitivity associated with larger \mathcal{C}_2 values in the Arrhenius law. According to the experimental findings shown in Fig. 4, the VB development rates among different cutting speeds exhibit larger variations compared to that of KT in Ti6Al4V cutting. As a result, if the Usui wear model is to be calibrated, the fitted \mathcal{C}_2 coefficient is likely to be higher for the flank face than for the rake face.



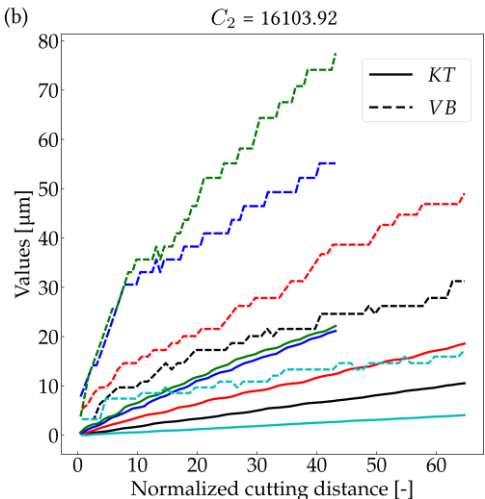


Fig. 7: Comparison of simulated KT and VB values in cutting Ti6Al4V material at different cutting speeds with the Usui wear model, using two different coefficients of (a) $C_2 = 5000$ and (b) $C_2 = 16103.92$ respectively.

4.2 Wear model calibration using wear progression simulation results

In this section, the rates of *KT* and VB from wear progression simulations are used to calibrate wear model constants. The model calibration contains two steps:

Step 1: Identification of C2

The identification of \mathcal{C}_2 relies on the established relationship between \mathcal{C}_2 and the relative change in wear rates at different cutting speeds. The wear rates from both simulation and experiment at the lowest tested cutting speed, i.e. 150 m/min, are chosen as the reference \dot{w}'_0 , and the wear rates \dot{w}' at other cutting speeds are normalized by computing their ratios relative to these reference values. The results are shown in Fig. 8, where the ratios \dot{w}'/\dot{w}'_0 are plotted against \mathcal{C}_2 and v_c . Note that w' denotes wear indicators such as KT and VB, which differ from the local wear rate predicted by wear models.

Based on this simulated wear rate data, two distinct interpolation approaches are proposed to characterize the wear rate map $\frac{w'}{w'_0} \sim f(\mathcal{C}_2, v_c)$:

· Physical assumption approach:

This approach involves computing the relative wear rate by directly applying the Usui wear model. A straightforward model is proposed as follows:

$$\begin{cases} \frac{w'}{w'_0} \sim f(C_2, v_c) = \frac{v_c}{v_{c,0}} \frac{p}{p_0} \exp(-\left[\frac{C_2}{T} - \frac{C_2}{T_0}\right]) \\ T = A_1 + A_2 v_c^{A_3} \\ p = 1 + A_4 \ln \frac{v_c}{A_5} \end{cases}$$
(4)

in which the temperature is assumed based on a power law within the tested cutting speeds, while the simplification $\sigma_n \propto p$ uses the strain rate hardening term in the JC model (Eq. (2)). Consequently, the model contains five unknown parameters, denoted A_1 to A_5 , which need to be identified through regression analysis.

· Polynomial fitting:

$$\frac{w'}{w'_0} \sim f(C_2, v_c) = \sum_{k=0}^{p'} \sum_{i+j \le k} A_{i,j}^k v_c^i C_2^j$$
 (5)

where p' denotes the order of polynomials. In this study, fifth-degree polynomials are used, requiring the fitting of 21 unknown constants $A_{i,j}^k$.

As indicated by the coefficient of determination \mathbb{R}^2 listed in Tab. 3, the polynomial fitting provides a more accurate representation of the wear rate map compared to models based on physical assumptions. Using the polynomial fitting results of the simulated wear map, the effective \mathcal{C}_2 parameters for the experimental wear models can be obtained through interpolation. As shown in Tab. 3, the obtained \mathcal{C}_2 values for the flank wear land are higher than those for crater wear. This is consistent with the hypothesis presented in Section 2 that fundamentally different wear mechanisms may govern the rake and flank faces.

Tab. 3: Calibrated Usui wear model coefficients.

Surface	$\frac{\dot{w}'}{\dot{w}'_0} \sim f(\mathcal{C}_2, v_c)$	$C_1 \left[\frac{1}{GPa} \frac{\mu m}{m} \right]$	C ₂ [-]
rake	Physical based ($R^2 = 0.9932$)	$4021.48 \ (R^2 = 0.9808)$	$10456.69 (R^2 = 0.9998)$
	Polynomial based ($R^2 = 0.9973$)	$802.42 (R^2 = 0.9885)$	$8481.57 (R^2 = 0.9952)$
clearance	Physical based ($R^2 = 0.9954$)	$685672.95 (R^2 = 0.8201)$	$15909.42 (R^2 = 0.9818)$
	Polynomial based ($R^2 = 0.9981$)	$1541250.64 (R^2 = 0.7950)$	$16977.63 (R^2 = 0.9268)$

Step 2: Identification of C₁

After determining the C_2 parameters, several methods can be used to identify \mathcal{C}_1 . One option involves computing intermediate variables such as σ_n , v_{rel} and T through a least square fit based on the sensitivity analysis results shown in Fig. 7, and subsequently deriving C_1 from these intermediate values. However, as C_1 is a linear factor in the wear model, its accuracy strongly depends on the precision of these intermediate values especially the temperature. To ensure robustness, a simpler approach is used: for a given C_2 , wear simulation is conducted under a selected cutting speed, and the resulting wear rate is used to calculate C_1 . The results of C_1 are listed in Tab. 3 as well. Notably, the R^2 values associated with rake face wear are significantly higher than those for flank face wear. A likely reason is the challenges introduced by the small cutting edge radius, for which a even finer particle resolution is required.

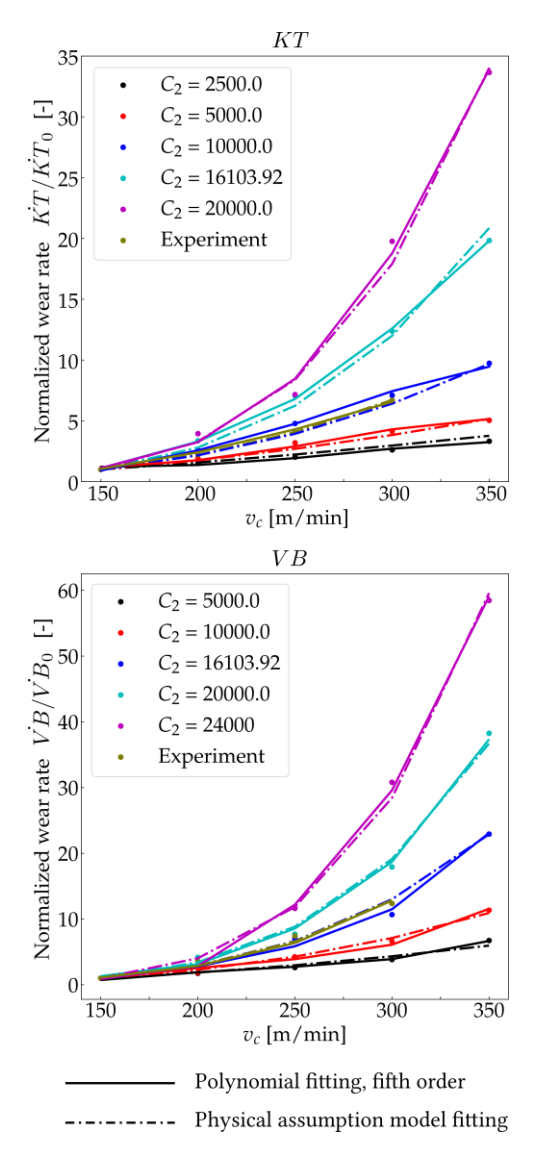


Fig. 8: Identification of C_2 coefficient in the Usui wear model using wear rate map $\frac{w'}{w'_0} \sim f(C_2, v_c)$. The parameters for crater wear and flank wear land are fitted separately.

The calibrated wear models are applied in wear progression simulations to verify their predictive accuracy, and the comparison between experimental wear indicators and simulated results is presented in Fig. 9. To minimize the effect of plastic deformation, the *KT* data has been adjusted

by subtracting the intersection point of the fitted curve on the KT axis in Fig. 3 (a) for each cutting speed. Overall, the simulated progression of KT closely aligns with experimental trends, indicating that plastic deformation predominantly occurs during the initial stages of continuous cutting. Regarding VB, although the general trend in wear rates is consistent with experimental observations, the prediction accuracy is lower compared to that of KT. One possible reason is that the initial rapid wear caused by cutting edge deformation cannot be captured in the current simulation framework. Despite this limitation, the reasonably good agreements particularly for crater wear support the validity of the proposed calibration method.

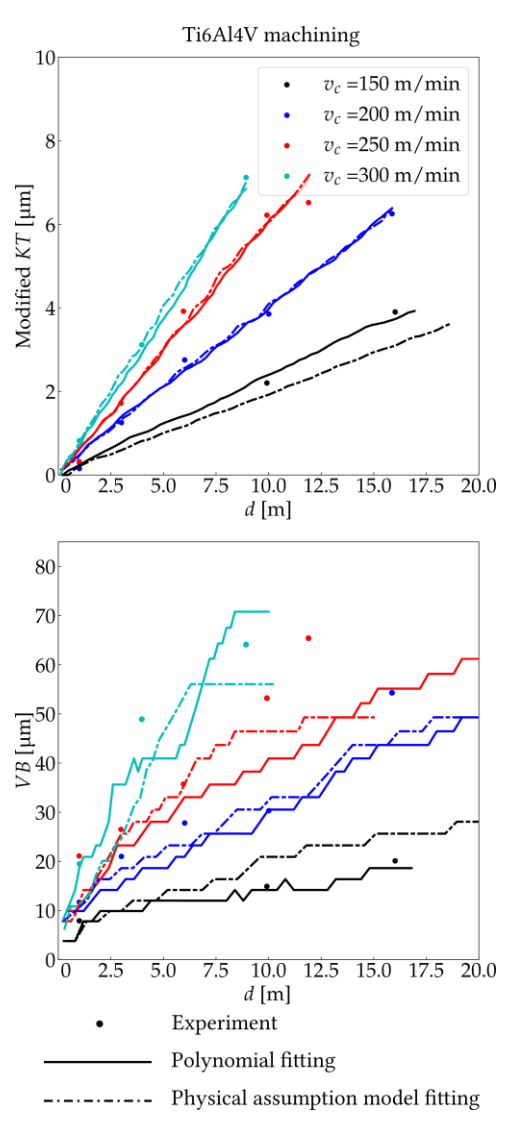


Fig. 9: Comparison of wear indicators KT and VB between experimental and simulation results using wear models from calibration.

5 CONCLUSION

This study employs a hybrid SPH-FEM cutting simulation method with integrated wear algorithms to investigate tool wear behavior and calibrate wear models for uncoated carbide tools during Ti6Al4V machining.

Experimental observations reveal distinct wear mechanisms on the rake and flank faces of the carbide tool. Diffusion- and oxidation-assisted attrition dominates the rake face, while mechanical wear prevails on the flank face

with minimal diffusion involvement. Wear simulations based on the Usui model show that higher Arrhenius coefficients increase the sensitivity of wear rates to cutting speed. Building on this insight, a new wear model calibration method is proposed using a wear rate map that links variations in wear rate across different cutting speeds to the Arrhenius coefficient. This approach enables effective identification of model parameters and supports reasonable prediction of crater depth and flank wear land width. The calibrated model further confirms the suitability of the Usui wear model for representing tool wear behavior in titanium alloy machining.

Importantly, the calibrated wear models are specific to the batches of workpiece materials and cutting inserts used in this study. The predictive accuracy of the calibrated models thus may decline when applied to different tool—workpiece combinations due to variations in tool manufacturing, carbide grain size, cobalt content, residual stresses, and other influencing factors. However, the model identification approach shows potential for broader applicability. Since the wear rate map depends solely on the simulation setup, it can be reused to estimate tool wear for different tool—workpiece pairs with minimal experimental effort. With just a few cutting tests, the wear progression can be predicted across a wider range of process parameters. Nevertheless, further validation is required to confirm the robustness and generalizability of this approach.

6 REFERENCES

[Attanasio 2010] Attanasio, A., Ceretti, E., Fiorentino, A., Cappellini, C.R.I.S.T.I.A.N. and Giardini, C. Investigation and FEM-based simulation of tool wear in turning operations with uncoated carbide tools. Wear, 2010, Vol.269, No.5-6, pp.344-350. ISSN 0043-1648

[Bencheikh 2020] Bencheikh, I., Nouari, M. and Bilteryst, F. Multi-step simulation of multi-coated tool wear using the coupled approach XFEM/multi-level-set. Tribology International, 2020, Vol.146, pp.106034. ISSN: 0301-679X

[Binder 2017] Binder, M., Klocke, F. and Döbbeler, B., 2017. An advanced numerical approach on tool wear simulation for tool and process design in metal cutting. Simulation modelling practice and theory, 2017, Vol.70, pp.65-82. ISSN 1569-190X

[daSilva 2019] da Silva, L.R., da Silva, O.S., dos Santos, F.V., Duarte, F.J. and Veloso, G.V. Wear mechanisms of cutting tools in high-speed turning of Ti6Al4V alloy. The International Journal of Advanced Manufacturing Technology, 2019, Vol.103, pp.37-48. ISSN 0268-3768

[Davies 2007] Davies, M.A., Ueda, T., M'saoubi, R., Mullany, B. and Cooke, A.L. On the measurement of temperature in material removal processes. CIRP annals, 2007, Vol.56, No.2, pp.581-604. ISSN 0007-8506

[Haddag 2013] Haddag, B. and Nouari, M. Tool wear and heat transfer analyses in dry machining based on multisteps numerical modelling and experimental validation. Wear, 2013, Vol.302, pp.1158-1170. ISSN 0043-1648

[Klippel 2021] Klippel, H. Constitutive equations for simulation of metal cutting with meshless methods on GPU. ETH Zurich, PhD Thesis, 2021.

[Lindvall 2021] Lindvall, R., Lenrick, F., M'Saoubi, R., Ståhl, J.E. and Bushlya, V. Performance and wear mechanisms of uncoated cemented carbide cutting tools in Ti6Al4V machining. Wear, 2021, Vol.477, p.203824. ISSN 0043-1648

[Lorentzon 2008] Lorentzon, J., Järvstråt, N. Modelling tool wear in cemented-carbide machining alloy 718. International Journal of Machine Tools and Manufacture, 2008, Vol.48, No.10, pp.072-1080. ISSN 0890-6955

[Malakizadi 2016] Malakizadi, A., Gruber, H., Sadik, I. and Nyborg, L. An FEM-based approach for tool wear estimation in machining. Wear, Vol. 368, pp.10-24. ISSN 0043-1648

[Meier 2020] Meier, L. Developing Metalworking Fluids for Titanium Cutting. ETH Zurich, PhD Thesis, 2020.

[Ozel 2010] Özel, T., Sima, M., Srivastava, A.K. and Kaftanoglu, B. Investigations on the effects of multi-layered coated inserts in machining Ti–6Al–4V alloy with experiments and finite element simulations. CIRP annals, 2010, Vol.59, No.1, pp.77-82. ISSN 0007-8506

[Usui 1984] Usui, E., Shirakashi, T. and Kitagawa, T. Analytical prediction of cutting tool wear. Wear, 1984, Vol.100, pp.129-151. ISSN 0043-1648

[Röthlin 2019] Röthlin, M. Meshless software tool to simulate metal cutting operations by employing contemporary numerical methods. ETH Zurich, PhD Thesis, 2019.

[Schulze 2011] Schulze, V. and Zanger, F. Development of a simulation model to investigate tool wear in Ti-6Al-4V alloy machining. Advanced materials research, 2011, Vol.223, pp.535-544. ISSN 1662-8985

[Wyen 2012] Wyen, C.F., Knapp, W. and Wegener, K. A new method for the characterisation of rounded cutting edges. The International Journal of advanced manufacturing technology, 2012, Vol.59, pp.899-914. ISSN 0268-3768

[Xie 2005] Xie, L.J., Schmidt, J., Schmidt, C. and Biesinger, F. 2D FEM estimate of tool wear in turning operation. Wear, 2005, Vol.258, No.10, pp.1479-1490. ISSN 0043-1648

[Yen 2002] Yen, Y.C., Söhner, J., Weule, H., Schmidt, J. and Altan, T. Estimation of tool wear of carbide tool in orthogonal cutting using FEM simulation. Machining science and technology, 2002, Vol.6, No.3, pp.467-486. ISSN 1091-0344

[Zanger 2013] Zanger, F. and Schulze, V. Investigations on mechanisms of tool wear in machining of Ti-6Al-4V using FEM simulation. Procedia CIRP, 2013, Vol.8, pp.158-163. ISSN 2212-8271

[Zhang 2009] Zhang, S., Li, J.F., Deng, J.X. and Li, Y.S. Investigation on diffusion wear during high-speed machining Ti-6Al-4V alloy with straight tungsten carbide tools. The International Journal of Advanced Manufacturing Technology, 2009, Vol.44, pp.17-25. ISSN 0268-3768

[Zhang 2023a] Zhang, N., Klippel, H., Kneubühler, F., Afrasiabi, M., Röthlin, M., Kuffa, M., Bambach, M. and Wegener, K. Study on the effect of wear models in tool wear simulation using hybrid SPH-FEM method. Procedia CIRP, 2023, Vol.117, pp.414-419. ISSN 2212-8271

[Zhang 2023b] Zhang, N., Klippel, H., Afrasiabi, M., Röthlin, M., Kuffa, M., Bambach, M. and Wegener, K., 2023. Hybrid SPH-FEM solver for metal cutting simulations on the GPU including thermal contact modeling. CIRP Journal of Manufacturing Science and Technology, 2024, Vol.41, pp.311-327. ISSN 1755-5817

[Zhang 2024] Zhang, N. SPH-FEM Modeling of Ti6Al4V Cutting Process: From Contact Establishment to Tool Wear Simulation. ETH Zurich, PhD Thesis, 2024